Isotopic evidence of multiple controls on atmospheric oxidants over climate transitions

Authors: Lei Geng[1,2,3], Lee T. Murray[4], Loretta J. Mickley[5], Pu Lin[6], Qiang Fu[1], Andrew J. Schauer[7], Becky Alexander[1]*

[1]Department of Atmospheric Sciences, University of Washington, Seattle, WA, 98195, USA

[2]Univ. Grenoble-Alpes & CNRS, LGGE, F-38000, Grenoble, France

[3]School of Earth and Space Sciences, University of Science and Technology of China, Hefei, 230026, Anhui, China

[4]Department of Earth and Environmental Sciences, University of Rochester, Rochester, NY, USA

[5]School of Engineering and Applied Sciences, Harvard University, Cambridge, MA, USA

[6]Program in Atmospheric and Oceanic Sciences, Princeton University, Princeton, New Jersey, USA

[7]Department of Earth and Space Sciences, University of Washington, Seattle, WA, 98195, USA

*Corresponding author email: beckya@uw.edu

The abundance of tropospheric oxidants (e.g., ozone (O_3) and HO_x ($OH + HO_2 + RO_2$)) determines the lifetimes of reduced trace gases such as methane (CH_4) and the production of particulate matter important for climate and human health. The response of tropospheric oxidants to climate change is poorly constrained due to large uncertainties in the degree to which processes that influence oxidants may change with climate[1] and to the lack of paleo-records of oxidants[2]. Current thinking is that temperature-dependent emissions of tropospheric O_3 precursors and water vapor abundance determines the climate response of oxidants, resulting in lower tropospheric O_3 in cold climates while HO_x remains relatively buffered[3]. Here we show ice-core observations demonstrating that the O_3/HO_x ratio increases in cold climates, the opposite of expectations. We hypothesize that the observed increase in O_3/HO_x in cold climates is driven by enhanced reactive halogen chemistry and/or enhanced stratosphere-to-troposphere transport (STT) of O_3. Reactive halogens influence the oxidative capacity of the troposphere directly as oxidants themselves and indirectly via their influence on O_3 and HO_x[4]. The strength of STT is largely controlled by the Brewer-Dobson Circulation (BDC)[5], which may be enhanced in colder climates due to a stronger meridional gradient of sea surface temperatures (SST)[6], with implications for the response of tropospheric oxidants[7] and stratospheric thermal and mass balance[8]. These two processes may represent important, yet relatively unexplored, climate feedback mechanisms during major climate transitions.

The oxygen-17 excess ($\Delta^{17}O = \delta^{17}O - 0.52 \times \delta^{18}O$) of ice-core nitrate is suggested to be one of the most promising proxies for reconstructing atmospheric oxidation capacity[2]. Greenland ice-core nitrate originates from deposition of atmospheric nitrate that formed in the northern hemisphere mid-latitude NO_x-source regions. Globally, atmospheric nitrate is formed mainly via

oxidation of NO_x by HO_x or O_3[9]. Oxidation of NO_x by reactive bromine (BrO) may also be important in the marine boundary layer[10] and during short-lived episodes such as polar ozone depletion events in Arctic spring[11]. O_3- and BrO-dominated reactions lead to high $\Delta^{17}O$ values in atmospheric nitrate, while HO_x-dominated reactions lead to low $\Delta^{17}O$ (*SI-S1*). The value of $\Delta^{17}O$ in ice-core nitrate ($\Delta^{17}O(NO_3^-)$) can thus provide information on these oxidants in past atmospheres, and is particularly sensitive to the ratio of $O_3/(HO_2 + RO_2)$ (*SI-S1*).

The glacial-interglacial ice-core record of $\Delta^{17}O(NO_3^-)$ (Figure 1a) displays a negative correlation with a proxy for local Greenland temperature ($\delta^{18}O(H_2O)$) ($r = -0.76$, $p < 0.01$, Figure 2a). Throughout the record, two samples fall within two Heinrich events (H1 ~16.8 ka and H2 ~ 23 ka) within or near the last glacial maximum (LGM, 19-23 ka BP)[12]. These two samples are in glacial climate conditions analogous to that in the LGM. We use the mean $\Delta^{17}O(NO_3^-)$ of these two samples to represent glacial $\Delta^{17}O(NO_3^-)$, which is (35.5 ± 0.7) ‰. Comparing the glacial $\Delta^{17}O(NO_3^-)$ to the mean of the four Holocene samples ($\Delta^{17}O(NO_3^-)$ =29.4 ± 0.7) ‰) yields a glacial-Holocene difference of ~ 6.2 ‰. The high resolution record of $\Delta^{17}O(NO_3^-)$ over two abrupt climate change events (Dansgaard–Oeschger (D-O) 12 and 13, Figure 1b) shows that $\Delta^{17}O(NO_3^-)$ responds rapidly to abrupt warming and cooling. In particular, immediately following the abrupt warming (~10 ºC increase in ~100 years in Greenland[12]) from GS-13 (Greenland Stadial 13, the cold phase of D-O 13) to GI-12 (Greenland Interstadial 12, the warm phase of D-O 12), $\Delta^{17}O(NO_3^-)$ decreased by (2.3 ± 0.2) ‰, a temperature-dependent response in the same direction as that on the glacial-interglacial timescale (Figure 1&2). Closer evaluation of the relationship between $\Delta^{17}O(NO_3^-)$ and temperature over this period reveals two regimes (Figure 2b). During the relatively warm period (43.9 - 45.4 ka B.P., i.e., GS-12 and the onset of its cooling), $\Delta^{17}O(NO_3^-)$ decreases moderately with decreasing temperature ($r = 0.40$, $p < 0.01$),

opposite to the trend observed on the glacial-interglacial timescale. In contrast, during the relatively cold periods of these two D-O events, $\Delta^{17}O(NO_3^-)$ increases strongly with decreasing temperature ($r = -0.82$, $p < 0.01$), similar to the direction of the trend on the glacial-interglacial timescale. We note this two-regime relationship observed in the D-O events may also exist over the glacial-interglacial cycle, but is impossible to statistically extract with the limited sample size we have over this time period.

ICECAP (ICE age Chemistry And Proxies) model[3] results (Methods) show decreases in tropospheric O_3 and ($HO_2 + RO_2$) abundances in cold climates compared to warm climates throughout the northern mid- to high-latitudes (Figure 3a and 3b). The modeled fraction of NO oxidized by O_3 (vs. $HO_2 + RO_2$ oxidation) in NO_x cycling (represented by the *A*-value, *SI-S1*), which explicitly determines $\Delta^{17}O(NO_2)$ and thus two-thirds of $\Delta^{17}O(NO_3^-)$ (*SI-S1.1*), also decreases in colder climates (Figure 3c). This suggests that changes in $O_3/(HO_2 + RO_2)$ ratio (Figure 3d) driven by temperature-dependent emissions of tropospheric O_3 precursors tend to lower $\Delta^{17}O(NO_3^-)$ in the glacial period compared to the Holocene, opposite to the observations.

Oxidation of NO_2 to HNO_3 (e.g., OH vs. O_3 oxidation) determines one-third of $\Delta^{17}O(NO_3^-)$ and may also vary with climate (*SI-S2*). Using ICECAP, we find that climate-driven changes in the oxidation of NO_2 to HNO_3 tend to lower $\Delta^{17}O(NO_3^-)$ in colder climates, except for changes in $BrONO_2$ hydrolysis. In ICECAP, the relative importance of nitrate formation via $BrONO_2$ hydrolysis in cold climates increases due to modeled higher glacial BrO concentrations relative to the Holocene (*SI-S1.2*). Increased BrO in the model is primarily driven by decreases in glacial HO_2 which is the largest sink of BrO_x (= Br + BrO). Increases in reactive Br production from increased HOBr photolysis due to reductions in other HOBr loss pathways (e.g., wet deposition) and increased polar photolysis rates also play a role[3]. Modeled changes in $BrONO_2$ hydrolysis

alone tend to increase glacial $\Delta^{17}O(NO_3^-)$ by 1.0 - 2.5 ‰. However, given the modeled lowered glacial *A*-value, $\Delta^{17}O(NO_3^-)$ in the LGM decreases by 2.5 - 3.3 ‰ compared to the Holocene. With this lower *A*-value, in order for increases in $BrONO_2$ hydrolysis to explain the magnitude of the observed glacial-interglacial change in $\Delta^{17}O(NO_3^-)$, such hydrolysis must account for 70 - 82 % of total nitrate production in the northern mid- to high-latitudes in the glacial period. $BrONO_2$ hydrolysis contributes only 20 ± 10 % to total nitrate production in high halogen environments (i.e., tropical marine boundary layer) in the present day atmosphere[10]. In the polar regions after polar sunrise when O_3 depletion events occur[13], $BrONO_2$ hydrolysis may dominate local nitrate production[11]. However, these short-lived episodes are constrained to polar springtime and do not represent the major nitrate production pathways over the larger spatial and temporal scales recorded in Greenland ice cores. The relative importance of $BrONO_2$ hydrolysis for nitrate production may be underestimated by ICECAP due to missing sources of halogens, such as the sea-ice source (*SI-S1.2*). No model studies have yet investigated the climate sensitivity of reactive halogen chemistry.

Modeling studies suggest an increase in STT of O_3 in the glacial climate driven by an enhanced BDC[6,14], which would tend to increase $\Delta^{17}O(NO_3^-)$ by increasing the concentration of tropospheric O_3, qualitatively consistent with the observations. The BDC is characterized by tropospheric air entering the stratosphere in the tropics and moving poleward before descending in the extra-tropics[5]. The BDC is comprised of a shallow branch that passes through the lowermost stratosphere and re-enters the troposphere in the subtropics and mid-latitudes, and a deep branch that rises to the upper stratosphere before descending in mid- and high-latitudes[15]. Enhanced STT mass exchange driven by a stronger BDC can therefore lead to enhanced tropospheric ozone in the mid- to high-latitudes[7]. Modeled increases in glacial STT are driven by

111 increased SST gradients between the tropics and mid- to high-latitudes during glacial periods
112 relative to the present, which acts to increase vertical wave propagation in the mid-latitudes
113 despite lower greenhouse gas (GHG) levels [6]. This is consistent with *Olsen et al.*[16] who found
114 that the BDC intensifies in response to a stronger SST gradient from the tropics through the mid-
115 latitudes in model simulations of the recent past, with or without an increasing atmospheric GHG
116 burden. In addition, although the total stratospheric O_3 column abundance is predicted to increase
117 only by a few percent in the LGM due to a warmer stratospheric temperature (radiative influence)
118 and the altered atmospheric composition and dynamics compared to the Holocene[6], the
119 lowermost stratospheric ozone in the mid- to high-latitudes may have been further enhanced by
120 an acceleration of the BDC. As a result, STT may have been stronger in the glacial period
121 compared to the Holocene, leading to regional increases in tropospheric O_3, particularly in the
122 northern hemisphere as predicted by global climate model simulations[3,6].

123 A stronger STT flux of O_3 tends to increase $\Delta^{17}O(NO_3^-)$ through increasing the relative
124 importance of O_3 in the oxidation of NO and NO_2. Increases in O_3 abundance will also tend to
125 increase reactive halogen abundance[17] and potentially the importance of $BrONO_2$ hydrolysis for
126 the formation of nitrate, in addition to increasing the importance of nighttime relative to daytime
127 nitrate production (*SI-S2*). Taking all of these reactions into account, we estimate that in the
128 northern mid-to high-latitude troposphere, the tropospheric abundance of stratospheric-sourced
129 O_3 in the glacial climate would need to increase by 118 - 252 % relative to the Holocene, in order
130 to explain the observed 6.2 ‰ increase in $\Delta^{17}O(NO_3^-)$. Because reactive halogen chemistry in the
131 LGM may be underestimated by ICECAP (*SI-S3*), these values reflect the high-end possible
132 change in STT of O_3 in the LGM, and are much higher than the model-simulated ~ 11% increase
133 in the downward transport of O_3 through the 200 mbar level in the extratropics from the

Holocene to LGM[6]. We note that increases in stratospheric-sourced O_3 by STT flux may be a result of a variety of processes, caused not only by an enhanced BDC but also increased stratospheric O_3 abundance due to lower CH_4 and N_2O abundances in the glacial climate, and/or increases in synoptic-scale processes such as tropopause folding events[18-19]. More research is required to examine the causes, and to assess the magnitude, of potential changes in STT in the glacial climate.

The response of $\Delta^{17}O(NO_3^-)$ to temperature during the abrupt warming and cooling transitions of the D-O events (Figures 1b, 2b) is also consistent with the effect of variations in meridional SST gradient on the strength of the BDC and STT flux of O_3. The temperature changes over a D-O event are associated with variations in the strength of the Atlantic Meridional Overturning Circulation (AMOC)[20-21]. The AMOC impacts the meridional gradient of SST in the northern hemisphere[22], with stronger AMOC resulting in weaker SST gradient, and vice versa. The latter in turn leads to changes in the BDC and thus STT[16]. The rapid resumption of the AMOC during the abrupt warming of a D-O event[20-21] suggests a rapid slowdown of the BDC and STT, leading to decreases in tropospheric O_3 and thus $\Delta^{17}O(NO_3^-)$ in the northern mid- to high-latitudes. In contrast, during the abrupt cooling of a D-O event, the AMOC rapidly declines[20-21] which may lead to rapid increases in the BDC and STT, resulting in increases in tropospheric O_3 and thus $\Delta^{17}O(NO_3^-)$. Changes in the abundance of reactive halogens via e.g., changes in the sea-ice source may also impact $\Delta^{17}O(NO_3^-)$ during abrupt climate changes, similar in direction to changes on the glacial-interglacial timescale.

During the smaller, more gradual climate changes in D-O 12 and 13, e.g., in the relatively warm period after the abrupt warming ~ 45.4 ka B.P, the observations indicate a positive relationship between $\Delta^{17}O(NO_3^-)$ and temperature. During this relatively warm period, variability

157 in the regional abundance of tropospheric O_3 is likely controlled by changes in temperature-
158 dependent emissions of O_3-precursor gases. Surface temperatures slowly decline during the
159 warm period, decreasing O_3 precursor emissions and tropospheric O_3 production. These
160 decreases tend to lower O_3/HO_x and thus $\Delta^{17}O(NO_3^-)$ as long as O_3 decreases more than HO_x,
161 consistent with our ICECAP model simulations (Figure 3d).

162 Our hypothesized response of the BDC to climate runs counter to the prediction of an
163 acceleration of the BDC in response to increasing GHG concentrations. However it is the
164 shallow instead of deep branch of the BDC that accelerates with increasing GHGs from the
165 recent past through the near future to 2100[15] due to increasing wave propagation from the
166 subtropical troposphere[23], which climate models robustly agree. Furthermore if future Arctic
167 amplification[24] offsets the effect of increasing GHGs on the meridional SST gradient[16] in the
168 northern hemisphere, model predictions of future intensification of the BDC in response to
169 increased GHGs[25] might be offset.

170 Increases in reactive halogen chemistry and the BDC might have important implications
171 for the oxidation capacity of the atmosphere in cold climates. Increases in the BDC in cold
172 climates would influence global tropospheric OH abundance by altering the spatial distribution
173 of stratospheric O_3 and thus UV-photolysis rates in the troposphere[3]. Enhanced transport of
174 stratospheric O_3 from the equator to the poles due to a stronger BDC lowers the overhead O_3-
175 column abundance in the tropics and elevates it in the polar regions[7]. All else being equal, this
176 will increase OH production in the tropics and decrease OH production in the mid- to high-
177 latitudes[3]. Changes in tropical OH are particularly important for understanding the global CH_4
178 budget because it is the OH abundance in the tropics that is most relevant for the CH_4 lifetime[26].
179 A stronger BDC in the last glacial period, which would reduce the tropical stratospheric ozone

column, should alone lead to enhanced tropical OH production and a shorter CH_4 lifetime. Enhanced reactive halogen chemistry in the LGM may also tend to influence the CH_4 lifetime directly via the chlorine radical sink[27] and indirectly via its influence on OH[4]. Climate-driven changes in the BDC and reactive halogen chemistry and their impacts on the oxidizing capacity of the atmosphere may need to be considered in order to reconcile global CH_4 variations during glacial-interglacial and abrupt climate changes[28].

1 Naik, V. *et al.* Preindustrial to present-day changes in tropospheric hydroxyl radical and methane lifetime from the Atmospheric Chemistry and Climate Model Intercomparison Project (ACCMIP). *Atmos. Chem. Phys.* **13**, 5277-5298, doi:10.5194/acp-13-5277-2013 (2013).

2 Alexander, B. & Mickley, L. Paleo-Perspectives on Potential Future Changes in the Oxidative Capacity of the Atmosphere Due to Climate Change and Anthropogenic Emissions. *Curr Pollution Rep*, 1-13, doi:10.1007/s40726-015-0006-0 (2015).

3 Murray, L. T. *et al.* Factors controlling variability in the oxidative capacity of the troposphere since the Last Glacial Maximum. *Atmos. Chem. Phys.* **14**, 3589-3622, doi:10.5194/acp-14-3589-2014 (2014).

4 Schmidt, J. A. *et al.* Modeling the observed tropospheric BrO background: Importance of multiphase chemistry and implications for ozone, OH, and mercury. *J. Geophys. Res.* **121**, 2015JD024229, doi:10.1002/2015jd024229 (2016).

5 Holton, J. R. *et al.* Stratosphere-Troposphere Exchange. *Rev. Geophys.* **33**, 403-439, doi:10.1029/95rg02097 (1995).

6 Rind, D., Lerner, J., McLinden, C. & Perlwitz, J. Stratospheric ozone during the Last Glacial Maximum. *Geophys. Res. Lett.* **36**, doi:10.1029/2009gl037617 (2009).

7 Hegglin, M. I. & Shepherd, T. G. Large climate-induced changes in ultraviolet index and stratosphere-to-troposphere ozone flux. *Nat Geosci* **2**, 687-691, doi:10.1038/NGEO604 (2009).

8 Butchart, N. The Brewer-Dobson circulation. *Rev. Geophys.* **52**, 157-184, doi:10.1002/2013RG000448 (2014).

9 Alexander, B. *et al.* Quantifying atmospheric nitrate formation pathways based on a global model of the oxygen isotopic composition ($\Delta^{17}O$) of atmospheric nitrate. *Atmos. Chem. Phys.* **9**, 5043-5056, doi:10.5194/acp-9-5043-2009 (2009).

10 Savarino, J. *et al.* Isotopic composition of atmospheric nitrate in a tropical marine boundary layer. *Proc. Natl. Acad. Sci.* **110**, 17668-17673, doi:10.1073/pnas.1216639110 (2013).

11 Morin, S., Savarino, J., Bekki, S., Gong, S. & Bottenheim, J. W. Signature of Arctic surface ozone depletion events in the isotope anomaly ($\Delta^{17}O$) of atmospheric nitrate. *Atmos. Chem. Phys.* **7**, 1451-1469, doi:10.5194/acp-7-1451-2007 (2007).

12 Alley, R. B. Wally Was Right: Predictive Ability of the North Atlantic "Conveyor Belt" Hypothesis for Abrupt Climate Change. *Annu. Rev. Earth Planet. Sci.* **35**, 241-272, doi:10.1146/annurev.earth.35.081006.131524 (2007).

13 Barrie, L. A., Bottenheim, J. W., Schnell, R. C., Crutzen, P. J. & Rasmussen, R. A. Ozone destruction and photochemical reactions at polar sunrise in the lower Arctic atmosphere. *Nature* **334**, 138-141, doi:10.1038/334138a0 (1988).

14 Rind, D., Chandler, M., Lonergan, P. & Lerner, J. Climate change and the middle atmosphere 5. Paleostratosphere in cold and warm climates. *J. Geophys. Res.* **106**, 20195-20212, doi:10.1029/2000jd900548 (2001).

15 Lin, P. & Fu, Q. Changes in various branches of the Brewer–Dobson circulation from an ensemble of chemistry climate models. *J. Geophys. Res.* **118**, 73-84, doi:10.1029/2012jd018813 (2013).
16 Olsen, M. A., Schoeberl, M. R. & Nielsen, J. E. Response of stratospheric circulation and stratosphere-troposphere exchange to changing sea surface temperatures. *J. Geophys. Res.* **112**, doi:10.1029/2006jd008012 (2007).
17 Sherwen, T., Evans, M. J., Carpenter, L. J., Schmidt, J. A. & Mickley, L. J. Halogen chemistry reduces tropospheric O3 radiative forcing. *Atmos. Chem. Phys.* **17**, 1557-1569, doi:10.5194/acp-17-1557-2017 (2017).
18 Sprenger, M., Wernli, H. & Bourqui, M. Stratosphere–Troposphere Exchange and Its Relation to Potential Vorticity Streamers and Cutoffs near the Extratropical Tropopause. *J. Atmos. Sci.* **64**, 1587-1602, doi:doi:10.1175/JAS3911.1 (2007).
19 Xie, B., Zhang, H., Wang, Z., Zhao, S. & Fu, Q. A modeling study of effective radiative forcing and climate response due to tropospheric ozone. *Adv Atmos Sci* **33**, 819-828, doi:10.1007/s00376-016-5193-0 (2016).
20 Knutti, R., Fluckiger, J., Stocker, T. F. & Timmermann, A. Strong hemispheric coupling of glacial climate through freshwater discharge and ocean circulation. *Nature* **430**, 851-856, doi:10.1038/nature02786 (2004).
21 McManus, J. F., Francois, R., Gherardi, J. M., Keigwin, L. D. & Brown-Leger, S. Collapse and rapid resumption of Atlantic meridional circulation linked to deglacial climate changes. *Nature* **428**, 834-837, doi:10.1038/Nature02494 (2004).
22 Persechino, A. *et al.* Decadal-timescale changes of the Atlantic overturning circulation and climate in a coupled climate model with a hybrid-coordinate ocean component. *Clim Dynam* **39**, 1021-1042, doi:10.1007/s00382-012-1432-y (2012).
23 Shepherd, T. G. & McLandress, C. A Robust Mechanism for Strengthening of the Brewer–Dobson Circulation in Response to Climate Change: Critical-Layer Control of Subtropical Wave Breaking. *J. Atmos. Sci.* **68**, 784-797, doi:10.1175/2010jas3608.1 (2011).
24 Miller, G. H. *et al.* Arctic amplification: can the past constrain the future? *Quaternary Sci Rev* **29**, 1779-1790, doi:10.1016/j.quascirev.2010.02.008 (2010).
25 Butchart, N. *et al.* Simulations of anthropogenic change in the strength of the Brewer-Dobson circulation. *Clim Dynam* **27**, 727-741, doi:10.1007/s00382-006-0162-4 (2006).
26 Holmes, C. D., Prather, M. J., Sovde, O. A. & Myhre, G. Future methane, hydroxyl, and their uncertainties: key climate and emission parameters for future predictions. *Atmos. Chem. Phys.* **13**, 285-302, doi:10.5194/acp-13-285-2013 (2013).
27 Allan, W., Struthers, H. & Lowe, D. C. Methane carbon isotope effects caused by atomic chlorine in the marine boundary layer: Global model results compared with Southern Hemisphere measurements. *J. Geophys. Res.* **112**, n/a-n/a, doi:10.1029/2006jd007369 (2007).
28 Brook, E. J., Sowers, T. & Orchardo, J. Rapid variations in atmospheric methane concentration during the past 110,000 years. *Science* **273**, 1087-1091, doi:10.1126/science.273.5278.1087 (1996).
29 Grootes, P. M. & Stuiver, M. Oxygen 18/16 variability in Greenland snow and ice with 10^{-3}- to 10^{5}-year time resolution. *J. Geophys. Res.* **102**, 26455-26470, doi:10.1029/97jc00880 (1997).
30 CLIMAP. The Surface of the Ice-Age Earth. *Science* **191**, 1131-1137, doi:10.1126/science.191.4232.1131 (1976).
31 Webb, R. S., Rind, D. H., Lehman, S. J., Healy, R. J. & Sigman, D. Influence of ocean heat transport on the climate of the Last Glacial Maximum. *Nature* **385**, 695-699, doi:10.1038/385695a0 (1997).

Figure Legends:

Figure 1. GISP2 ice-core record of $\Delta^{17}O(NO_3^-)$. $\Delta^{17}O(NO_3^-)$ from (a) the last 100 ka B.P., and (b) D-O 12 and 13. $\delta^{18}O(H_2O)$ is a local Greenland temperature proxy, varying similarly to Northern Hemisphere temperature on these timescale[12]. $\delta^{18}O(H_2O)$ in (a) with high resolution are from *Grootes and Stuiver*[29], and in (b) are measured from this study. Numbers in (a) represent D-O events, and H1-6 represent Heinrich events[12]. GI and GS in (b) represent Greenland interstadial and stadial stages. The shaded area in (b) indicates the warm period of D-O 12. The error bars represent one standard deviation of $\Delta^{17}O(NO_3^-)$ from triplicate measurements.

Figure 2. Relationship between measured $\delta^{18}O(H_2O)$ and $\Delta^{17}O(NO_3^-)$. $\Delta^{17}O(NO_3^-)$ during the glacial-interglacial period (a), and D-O 12 and 13 over 43-49 ka B.P. (b). Red in (b) represents observations during the relatively warm period (GI-12 and its onset of cooling during 43.9-45.4 ka B.P.) of D-O 12 and 13, while black represents the observations during the relatively cold period. The error bars of $\Delta^{17}O(NO_3^-)$ represent one standard deviation of each sample measured in triplicate. The linear regression equations, and the r and the *p* values, are shown in each figure.

Figure 3. ICECAP model results of zonal mean tropospheric oxidants in the Holocene and glacial climates. Zonal-mean O_3 concentrations (a), $HO_2 + RO_2$ concentrations (b), the A-value (c) and the $O_3/(HO_2 + RO_2)$ ratio (d) in the Northern mid- to high-latitudes are shown. Also shown is the relative difference between the glacial and Holocene. The glacial climate is represented by two different global temperature reconstruction scenarios, the warm LGM from CLIMAP[30] and the cold LGM from *Webb et al*.[31] These model results consider the impact of changes in precursor emissions and chemistry only.

Supplementary Information is available in the online version of the paper.

Acknowledgments: We acknowledge financial support from NSF awards AGS 1103163, PLR 1106317 and PLR 1244817 to B. Alexander, and award NSF-AGS 1102880 to L. J. Mickley and L. T. Murray. We want to thank the National Ice Core Laboratory for providing the GISP2 ice-core samples, and the GISP2 team for ice core drilling. We also want to thank our lab technician B. Vanden Heuvel for measurements of $\delta^{18}O(H_2O)$.

Author Contributions: B.A. conceived the study; L.G. performed the measurements, analyzed the experimental and model data, proposed the hypotheses and wrote the manuscript with B.A.; L.T.M constructed the ICECAP model under the supervision of L.J.M., and provided the model

results; L.T.M., P. L. and Q. F. contributed to the hypotheses; A. J. S. assisted with the laboratory work. All authors contributed to the data interpretation and writing.

Author Information: Reprints and permissions information is available at www.nature.com/reprints. The authors declare no competing financial interests. Readers are welcome to comment on the online version of the paper. Correspondence and requests for materials should be addressed to B.A. (beckya@uw.edu).

Methods

Sample collection and laboratory analysis

The samples are from the Greenland Ice Sheet Project 2 (GISP2, Summit, Greenland, 72.6 ºN, 38.5 ºW, 3200 m elevation, 0.24 m ice a^{-1} at present [32]) ice core. We collected 15 discrete samples (~2 kg of ice each) between 264 to 2735 meters depth covering the last glacial-interglacial cycle (~1 to 100 ka BP). Each sample spans ~50 cm depth, representing 2-200 years of snow accumulation. Another 112 continuous samples throughout the depth interval of 2310 to 2413 meters were collected, covering the D-O 12 and 13 cycles between 43-49 ka BP[29]. The length of each sample is 0.8-1.0 meter, representing ~50 years of snow accumulation. All samples were decontaminated by removing the surface layer (~0.5 cm) with a band saw in a cold room (-8 ºC) followed by rinsing with 18 MΩ/cm water. The samples were then placed in covered, pre-cleaned beakers and melted at room temperature in a clean, laminar-flow hood. After melting, nitrate in the discrete samples was concentrated using an ion chromatograph[33] and nitrate in the continuous samples was concentrated using the resin method[34].

In IsoLab (http://isolab.ess.washington.edu/isolab/) at the University of Washington, the concentrated samples were then measured for $\Delta^{17}O(NO_3^-)$ in triplicate using the bacterial denitrifier method with a gold tube[35] on a Delta Plus Advantage isotope ratio mass spectrometer. Briefly, denitrifying bacteria convert NO_3^- to N_2O which is decomposed to O_2 and N_2 in a heated gold tube at 800 ºC. The thermal products of O_2 and N_2 are separated by a gas chromatograph, followed by the measurement of the mass/charge (*m/z*) of 28 and 29 from N_2, and *m/z* of 32, 33 and 34 form O_2. The mass ratios of $^{33}O_2/^{32}O_2$ and $^{34}O_2/^{32}O_2$ are converted to atomic ratios of $^{17}O/^{16}O$ and $^{18}O/^{16}O$, respectively. The atomic ratios are then converted to delta notion, $\delta^{17}O$ and $\delta^{18}O$, with respect to Vienna Standard Mean Ocean Water (VSMOW), where δ =

335 $(^{x}O/^{16}O_{sample})/(^{x}O/^{16}O_{VSMOW}) - 1$ with x = 17 or 18. The $\delta^{17}O$ and $\delta^{18}O$ values are normalized to
336 the VSMOW scale using two international reference materials USGS34 ($\delta^{17}O$ = - 14.5 ‰, $\delta^{18}O$
337 = - 27.9 ‰) and USGS35 ($\delta^{17}O$ = 51.3 ‰, $\delta^{18}O$ = 57.5 ‰)[35], with a 1:1 mixture of USGS34
338 and USGS35 used as a quality control standard. The $\Delta^{17}O$ values are then calculated using the
339 linear approximation $\Delta^{17}O \approx \delta^{17}O - 0.52 \times \delta^{18}O$. The analytical uncertainty of $\Delta^{17}O(NO_3^-)$ was ±
340 0.1 ‰ based on repeated measurements of the quality control standard.
341 $\delta^{18}O(H_2O)$ of the 15 glacial-interglacial samples and the 112 samples over DO-12 and 13
342 events are also measured in IsoLab using a Cavity Ring-down Spectrometer[36] (Picarro L-2120i).
343 $\delta^{18}O(H_2O)$ is expressed relative to VSMOW using in-house reference waters that were
344 previously measured against VSMOW and SLAP (Standard Light Antarctic Precipitation)
345 international reference waters. The measured $\delta^{18}O(H_2O)$ of each sample is almost identical to the
346 averaged $\delta^{18}O(H_2O)$ over the same depth interval calculated from the high resolution data
347 reported by *Grootes and Stuiver*[29].

348 **The ICECAP model**

349 The ICECAP model is a climate-biosphere-chemistry modeling framework for simulating the
350 chemical composition of the atmosphere at and since the LGM[3]. In ICECAP, the climate is
351 simulated by the GISS ModelE, which is forced by reconstructed greenhouse gas levels, sea
352 surface temperatures, orbital parameters, topography, and sea ice coverage. The ModelE
353 meteorological fields are applied to two global vegetation models: BIOME4-TG[37] to determine
354 land cover characteristics and LPJ-LMfire[38] to calculate dry matter consumed by fires. Model-E
355 meteorology and the land cover products are then used to drive the GEOS-Chem Chemical
356 Transport Model (CTM) of tropospheric composition[3]. With this framework, we can test the
357 sensitivity of tropospheric oxidants to diverse controlling factors across a range of uncertainty.

ICECAP also simulates stratospheric O_3 using the Linoz linearized chemical scheme and an array of about 20 species in the stratosphere in order to account for the chemical fluxes, including O_3, across the tropopause. ICECAP predicts increased STT during the LGM relative to the Holocene in some regions of the Northern Hemisphere, qualitatively consistent with the observations. However, we have little confidence that the model captures the magnitudes of changes in STT across climate transitions. The simulations of the ICECAP model used are known to have a high bias in the polar stratosphere-to-troposphere air-mass flux, which leads to a large overestimation of the stratospheric ozone flux despite reasonable stratospheric ozone concentrations[3]. This is likely due to the relatively coarse vertical resolution of this version of ModelE, which provides the meteorology for use in GEOS-Chem. The coarse vertical resolution may also cause ModelE to not fully resolve features such as tropopause folding events that can contribute significantly to local stratosphere-troposphere exchange. The low vertical resolution in ModelE may also lead to bias in the wave propagation from the troposphere into the stratosphere. Furthermore, climate models lacking resolved mesosphere dynamics such as Model-E require parameterizations of the gravity wave drag force that drives the Brewer-Dobson Circulation (BDC). Previous studies have shown that the simulated stratospheric climate is sensitive to the choice of gravity wave drag parameterization in the model (*Alexander et al.*[39] and references therein). Such parameterization is employed to represent the small-scale gravity waves that transport momentum from the troposphere and surface to the middle atmosphere. These waves are small in scale and intermittent in occurrence, and have few observational constraints. The change of these gravity waves under different climate and surface orographies such as the LGM is even less constrained. Therefore, we don't use the ICECAP model to explicitly interpret the STT changes in this work.

For these reasons, we use ICECAP only to investigate the sensitivity of tropospheric O_3 and HO_x abundances to precursor emissions and chemistry and not to STT. We calculate tropospheric O_3 production in each climate regime according to their different vegetation, fire and lightning emission scenarios, and to their (RO_2+HO_2) abundances. This information is used to calculate the relative importance of O_3 versus (RO_2+HO_2) in NO_x cycling, which determines the $\Delta^{17}O$ value of NO_2 and largely that of NO_3^-. We also use ICECAP to estimate the glacial-interglacial changes in the relative importance of each oxidation pathway from NO_2 to NO_3^-, thereby determining the overall changes in $\Delta^{17}O(NO_3^-)$ that originates from tropospheric chemistry. These are detailed in *SI-S5&6*.

Data availability

The ice-core data that support the findings of this study are available from the NSF Arctic Data Center: https://arcticdata.io/catalog/#view/doi:10.18739/A23T0C

32 Cuffey, K. M. & Clow, G. D. Temperature, accumulation, and ice sheet elevation in central Greenland through the last deglacial transition. *J. Geophys. Res.* **102**, 26383-26396, doi:10.1029/96jc03981 (1997).

33 Geng, L. *et al.* Analysis of oxygen-17 excess of nitrate and sulfate at sub-micromole levels using the pyrolysis method. *Rapid Commun. Mass Spectrom.* **27**, 2411-2419, doi:10.1002/rcm.6703 (2013).

34 Geng, L. *et al.* On the origin of the occasional spring nitrate peak in Greenland snow. *Atmos. Chem. Phys.* **14**, 13361-13376, doi:10.5194/acp-14-13361-2014 (2014).

35 Kaiser, J., Hastings, M. G., Houlton, B. Z., Rockmann, T. & Sigman, D. M. Triple oxygen isotope analysis of nitrate using the denitrifier method and thermal decomposition of N_2O. *Anal. Chem.* **79**, 599-607, doi:10.1021/Ac061022s (2007).

36 Gupta, P., Noone, D., Galewsky, J., Sweeney, C. & Vaughn, B. H. Demonstration of high-precision continuous measurements of water vapor isotopologues in laboratory and remote field deployments using wavelength-scanned cavity ring-down spectroscopy (WS-CRDS) technology. *Rapid Commun. Mass Spectrom.* **23**, 2534-2542, doi:10.1002/rcm.4100 (2009).

37 Kaplan, J. O., Folberth, G. & Hauglustaine, D. A. Role of methane and biogenic volatile organic compound sources in late glacial and Holocene fluctuations of atmospheric methane concentrations. *Global Biogeochem. Cy.* **20**, doi:10.1029/2005GB002590 (2006).

38 Pfeiffer, M., Spessa, A. & Kaplan, J. O. A model for global biomass burning in preindustrial time: LPJ-LMfire (v1.0). *Geosci. Model Dev.* **6**, 643-685, doi:10.5194/gmd-6-643-2013 (2013).

39 Alexander, M. J. *et al.* Recent developments in gravity-wave effects in climate models and the global distribution of gravity-wave momentum flux from observations and models. *Q J Roy Meteor Soc* **136**, 1103-1124, doi:10.1002/qj.637 (2010).

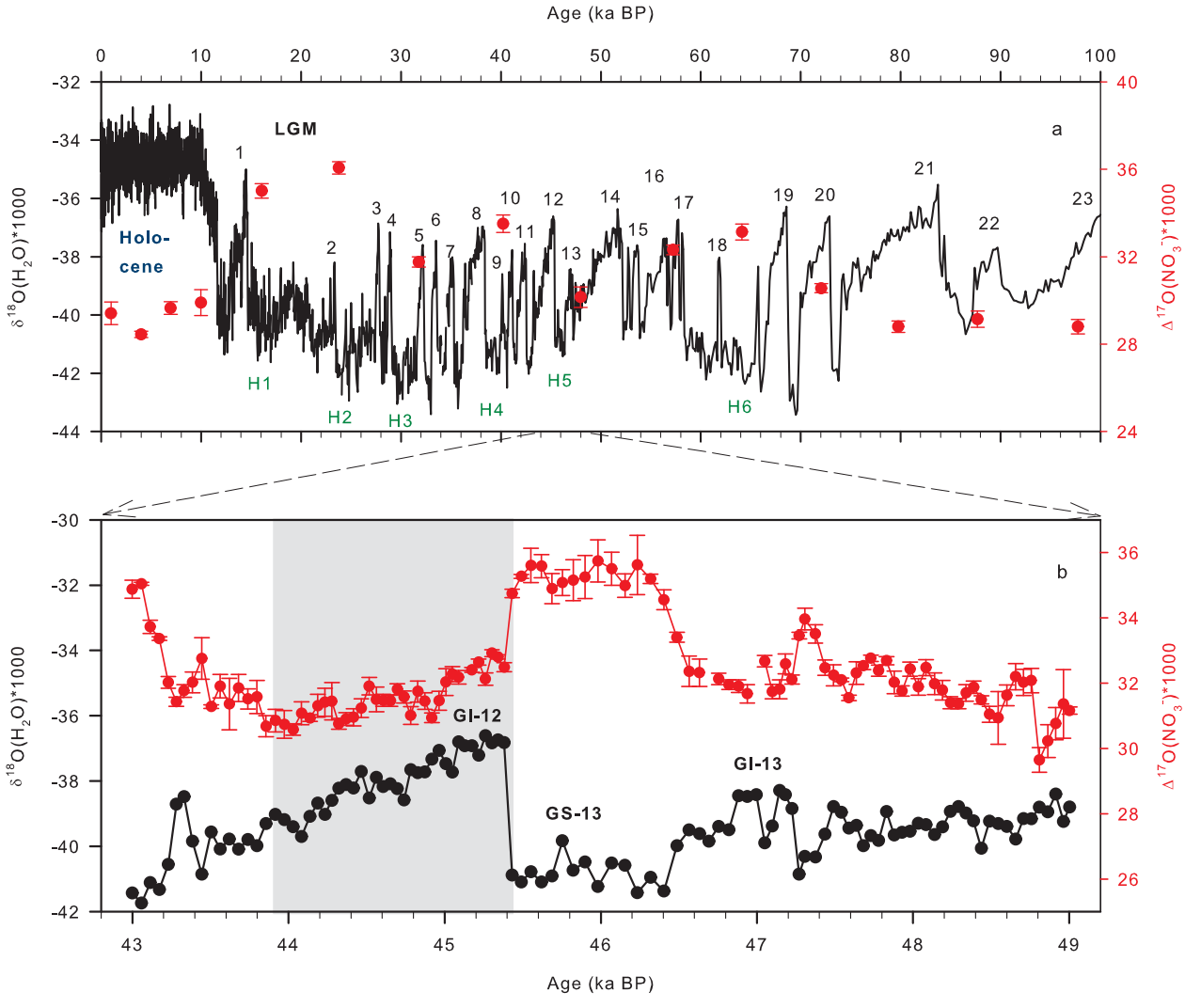
Age (ka BP)
0
10
20
30
40
50
60
70
80
90
100
-32
-34
-36
-38
-40
-42
-44
40
36
32
28
24
δ18O(H2O)*1000
Δ17O(NO3-)*1000
LGM
a
Holo-
cene
1
2
3
4
5
6
7
8
9
10
11
12
13
14
15
16
17
18
19
20
21
22
23
H1
H2
H3
H4
H5
H6
b
GI-12
GI-13
GS-13
-30
-32
-34
-36
-38
-40
-42
36
34
32
30
28
26
43
44
45
46
47
48
49
Age (ka BP)

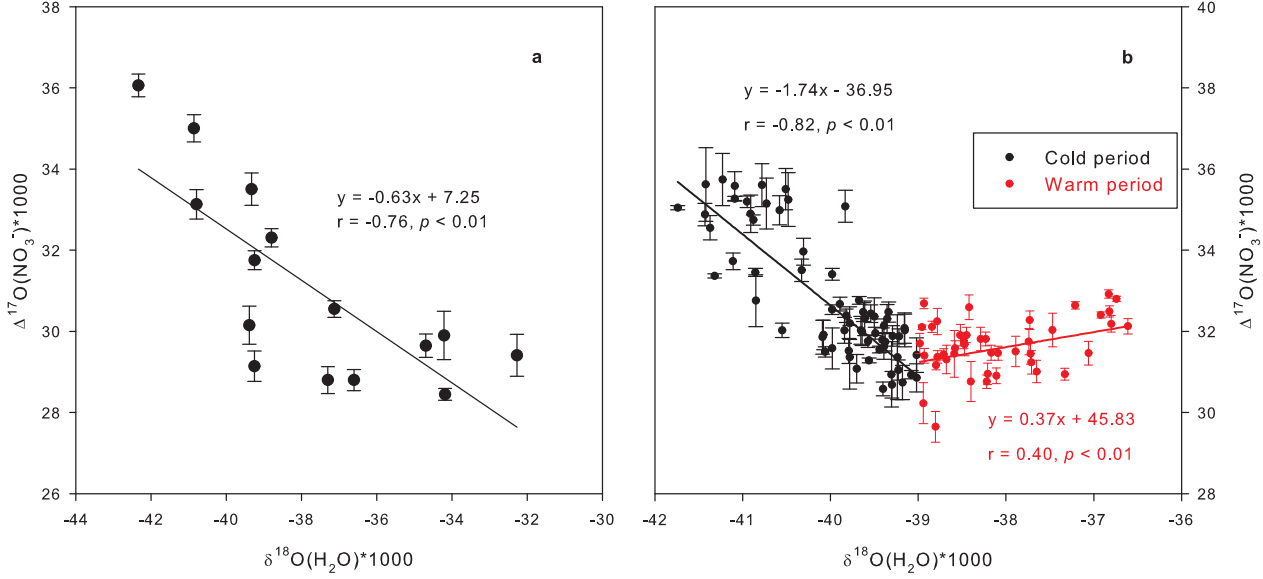
a
y = -0.63x + 7.25
r = -0.76, p < 0.01
Δ17O(NO3-)*1000
δ18O(H2O)*1000
b
y = -1.74x - 36.95
r = -0.82, p < 0.01
Cold period
Warm period
y = 0.37x + 45.83
r = 0.40, p < 0.01
Δ17O(NO3-)*1000
δ18O(H2O)*1000

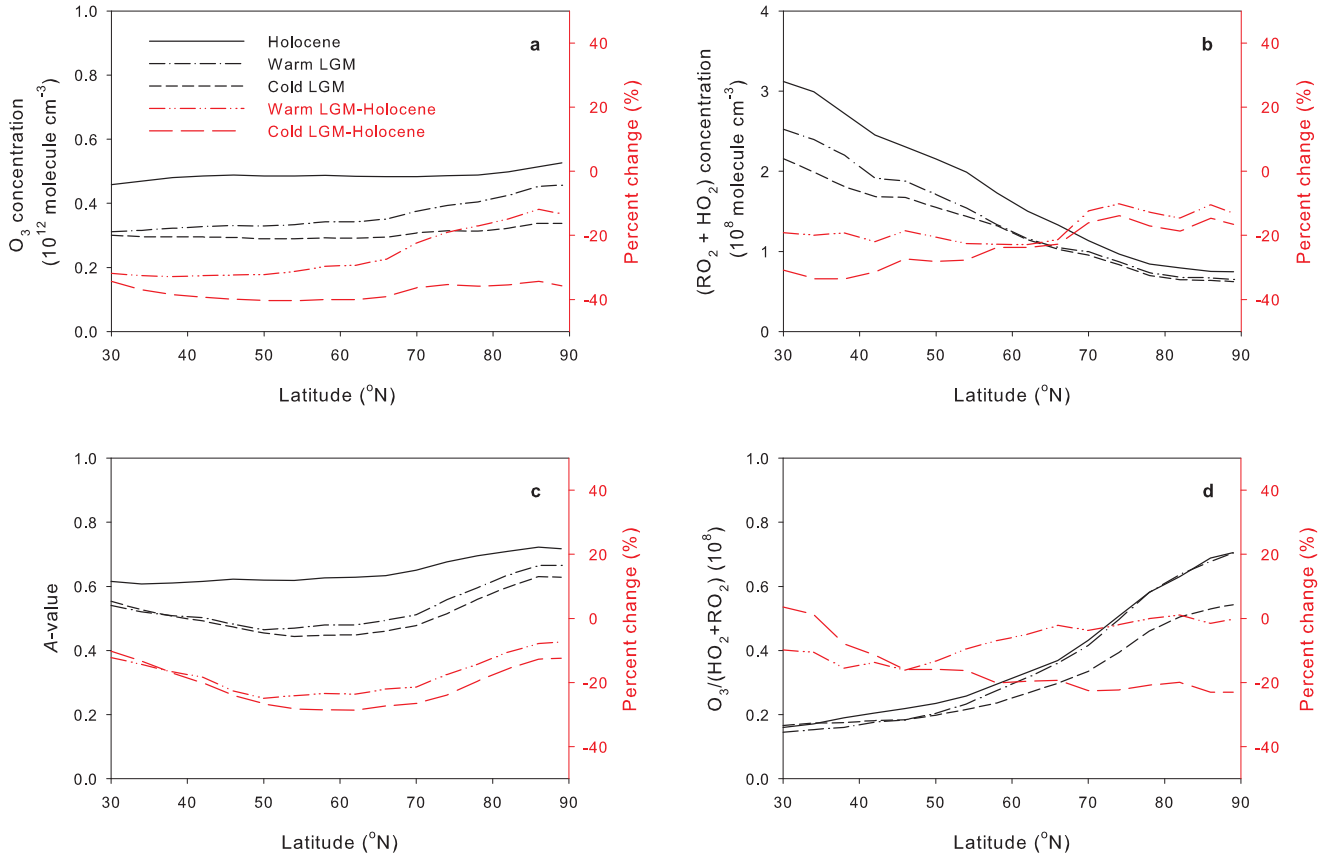
a
Holocene
Warm LGM
Cold LGM
Warm LGM-Holocene
Cold LGM-Holocene
O3 concentration (10^12 molecule cm^-3)
Percent change (%)
Latitude (°N)
b
(RO2 + HO2) concentration (10^8 molecule cm^-3)
Percent change (%)
Latitude (°N)
c
A-value
Percent change (%)
Latitude (°N)
d
O3/(HO2+RO2) (10^8)
Percent change (%)
Latitude (°N)

Isotopic evidence of multiple controls on atmospheric oxidants over climate transitions

Authors: Lei Geng[1,2,3], Lee T. Murray[4], Loretta J. Mickley[5], Pu Lin[6], Qiang Fu[1], Andrew J. Schauer[7], Becky Alexander[1]*

[1]Department of Atmospheric Sciences, University of Washington, Seattle, WA, 98195, USA

[2]Univ. Grenoble-Alpes & CNRS, LGGE, F-38000, Grenoble, France

[3]School of Earth and Space Sciences, University of Science and Technology of China, Hefei, 230026, Anhui, China

[4]Department of Earth and Environmental Sciences, University of Rochester, Rochester, NY, USA

[5]School of Engineering and Applied Sciences, Harvard University, Cambridge, MA, USA

[6]Program in Atmospheric and Oceanic Sciences, Princeton University, Princeton, New Jersey, USA

[7]Department of Earth and Space Sciences, University of Washington, Seattle, WA, 98195, USA

*Corresponding author email: beckya@uw.edu

Supplementary discussion

S1. Factors determining $\Delta^{17}O$ in atmospheric nitrate

Atmospheric nitrate is the oxidation product of NO_x ($NO_x \equiv NO + NO_2$). NO_x is emitted from natural sources including biomass burning, lightning and soil bioactivity, and anthropogenic sources mainly from fossil fuel combustion[40]. During NO_x cycling, NO is oxidized to NO_2 primarily by O_3, HO_2 and RO_2. Terminal reactions that oxidize NO_2 to HNO_3 are different between day- and nighttime. During the daytime, NO_2 is photolyzed to produce NO + O, or is oxidized to HNO_3 by OH. In the daytime, cycling of NO_x between NO and NO_2 is at least 3 orders of magnitude faster than its loss by oxidation to HNO_3, so that NO_x achieves isotopic equilibrium with O_3, HO_2, and RO_2[41]. At night, the oxidation of NO_2 by O_3 to form NO_3 is important for HNO_3 formation. NO_3 can then react with dimethyl sulphide (DMS) or volatile organic compounds (VOC) to form HNO_3, or with NO_2 to form N_2O_5 which hydrolyzes to HNO_3 on the surface of aerosols. In the present day, NO_2 + OH contributes to 76% of global, tropospheric nitrate formation, with N_2O_5 hydrolysis as the second largest contributor (18%)[41]. Reactive bromine (BrO) also plays a role in both NO_x cycling and nitrate formation in polar regions[42-43] and in the marine boundary layer[44], although its global importance is not well-quantified[41].

The O-17 excess ($\Delta^{17}O$) value of oxygen isotopes is a mass-independent fractionation signal created during O_3 formation and transferred to other oxygen-bearing compounds during oxidation reactions[45]. It is conventionally known that fractionation of isotopes in physical-chemical processes is mass-dependent, from which changes in isotopic ratios of polyisotopic elements (e.g., oxygen and sulphur) are scaled in proportion to their relative mass difference. Therefore, mass-dependent fractionation gives an approximate relationship of $\delta^{17}O \approx 0.52 \times$

$\delta^{18}O$. During the photochemical production of O_3, due to the asymmetric effect associated with the recombination of O_2 and O (intermediate products of O_3 formation)[46], the isotope fractionation deviates from the mass-dependent relationship, leading to an excess of O-17 which is calculated by $\Delta^{17}O = \delta^{17}O - 0.52 \times \delta^{18}O$. For most other physical and chemical processes, oxygen isotopes obey mass-dependent fractionation producing zero $\Delta^{17}O$, the $\Delta^{17}O$ value of most other oxygen-bearing molecules in the atmosphere is explicitly determined by the degree of the interactions between their precursors with O_3.

The $\Delta^{17}O$ of NO_2 ($\Delta^{17}O(NO_2)$) is determined by the relative abundance of $O_3/(HO_2 + RO_2)$ during NO_x cycling reactions, while the $\Delta^{17}O$ of nitrate ($\Delta^{17}O(NO_3^-)$) is determined by both $\Delta^{17}O(NO_2)$ and the oxidant (OH or O_3) involved in the oxidation of NO_2 to HNO_3[41]. If more O_3 is involved in the production of nitrate, higher $\Delta^{17}O$ values in nitrate will result. Because two thirds of oxygen atoms in nitrate is from NO_2, $\Delta^{17}O(NO_3^-)$ is most sensitive to the value of $\Delta^{17}O(NO_2)$, and hence the variability of $\Delta^{17}O(NO_3^-)$ is dominated by variability in the relative $O_3/(HO_2 + RO_2)$ abundance[47]. This makes $\Delta^{17}O(NO_3^-)$ a good proxy for the relative abundance of O_3 and $(HO_2 + RO_2)$. In contrast, $\delta^{18}O(NO_3^-)$ is influenced by the relative abundance of oxidants involved in nitrate formation and $\delta^{18}O$ of water. Unlike $\Delta^{17}O$, the $\delta^{18}O$ of oxidants and water varies over space and time. These multiple dependencies make $\delta^{18}O(NO_3^-)$ much more difficult to interpret as a proxy for oxidant levels. *Hastings et al.*[48] uses $\delta^{18}O(NO_3^-)$ to look for changes in nitrate formations pathways (day- vs. night-time reactions), rather than to explore changes in past oxidant levels. The former is possible because of the large difference between $\delta^{18}O$ of water (which determines $\delta^{18}O(OH)$, the main day-time oxidant) and O_3 (the main night-time oxidant).

The $\Delta^{17}O$ value of tropospheric O_3 is currently in debate. Measurements using nitrite-coated filters to collected tropospheric O_3 by *Vicars et al.*[49-50] suggest that $\Delta^{17}O$ of tropospheric O_3 is ~ 25 ‰. This is at the lower range of other observations[51], and is not consistent with the result of laboratory and model experiments by *Michalski et al.*[52] who suggest $\Delta^{17}O$ of O_3 is ~ 35 ‰. Because adopting the value of 35 ‰ predicts a better agreement between measured and modeled $\Delta^{17}O(NO_3^-)$ values in the global atmosphere, in this study, we use 35 ‰ as the $\Delta^{17}O$ value of O_3 when estimating $\Delta^{17}O(NO_3^-)$ in different climate using the ICECAP model.

In the following discussions, we utilize the ICECAP model to explore the effects of tropospheric precursor emissions and chemistry change on the NO_x cycling and terminal reactions from NO_2 to HNO_3 in different climates (i.e., Holocene and LGM), thereby discerning the causes of changes in $\Delta^{17}O(NO_3^-)$ from one climate to the other.

S1.1 The NO_x cycling

Globally, the value of $\Delta^{17}O(NO_2)$ is determined by the relative importance of O_3 versus RO_2 and HO_2 oxidation of NO to NO_2. Tropospheric O_3 production depends on emissions of precursor gases including VOCs, CO and NO_x that are sensitive to temperature and other meteorological conditions. Lower temperatures in colder climates will reduce O_3 precursor emissions[53-55], which tends to decrease global tropospheric O_3 production in the glacial period compared to the Holocene[54]. The response of the HO_x family to precursor emissions is more complicated. Production of HO_x is primarily sensitive to O_3 photolysis frequencies and water vapor abundances. The relative partitioning of HO_x between OH and (RO_2+HO_2) is controlled by the relative abundances of NO versus CO+VOCs. Therefore, variations in (RO_2+ HO_2) reflect the convolution of these parameters, and vary relatively independently from tropospheric O_3 itself[53]. Models generally predict higher OH in the glacial period compared to the Holocene[47],

especially in the high latitudes due to reduced sinks (CO and VOCs) and higher surface UV albedos caused by enhanced snow and ice cover[53]. The effect of changing OH alone on $\Delta^{17}O(NO_3^-)$ is considered to be relatively small, as the variability of $\Delta^{17}O(NO_3^-)$ is most sensitive to the relative abundances of O_3 and (HO_2 + RO_2).

In the polar regions, BrO can also be important over short time periods for oxidizing NO to NO_2, such as polar spring associated with ozone depletion events[42,56]. Because BrO is produced from Br reacting with O_3, during ozone depletion events, there is an anti-correlation between O_3 and BrO abundances[57]. BrO obtains its oxygen atom from O_3 and thus possesses and transfers the same $\Delta^{17}O$ to NO_2 when oxidizing NO as does O_3, making these two pathways isotopically indistinguishable. In the northern mid- to high-latitudes, the ICECAP model predicts that annual-mean BrO oxidation in NO_x cycling is less than 1 % in the Holocene, and ~2.2% and 1.4 % in the cold and warm LGM, respectively. Due to the small influence of BrO in NO_x cycling in all time periods in the ICECAP model, we ignore the effect of BrO in NO_x cycling in our analysis.

Using the ICECAP model, we estimate changes in tropospheric O_3 abundance due to changing O_3-precursor emissions and chemistry alone from the Holocene to the LGM (Figure 3). As expected, tropospheric O_3 abundance decreases in the glacial period due to reductions in temperature-dependent emissions of O_3-precursors. The ICECAP model also calculates decreases in tropospheric (HO_2 + RO_2) from the Holocene to the LGM (Figure 3b). The decreases in HO_2 are due both to reductions in primary HO_x production from reduced water vapor abundances in colder climates, as well as a shift of HO_x partitioning toward OH and RO_2 due to relative changes in NO_x, VOC, and CO abundances[53]. The decreases in modeled RO_2 in the glacial climates are mainly due to the reduction of VOCs.

The ratio of $O_3/(HO_2 + RO_2)$, which determines $\Delta^{17}O(NO_2)$, is plotted in Figure 3d. Although large spatial variability exists, in general the $O_3/(HO_2 + RO_2)$ ratio decreases in the LGM compared to the Holocene in the northern mid- to high-latitudes. In particular, in the northern mid- to high-latitudes (30 to 90 °N), the ratio decreases by 6.6 % and 15.6 % on average in the warm and cold LGM scenarios, respectively, compared to the Holocene. Based on the model predicted tropospheric *in-situ* O_3 and $(HO_2 + RO_2)$ abundances in the LGM and Holocene, we further calculate the conversion rates of NO to NO_2 via O_3, HO_2 and RO_2 oxidation, and the fraction of O_3 oxidation of NO in NO_2 formation in each climate. The latter explicitly determines $\Delta^{17}O(NO_2)$[41]. Following *Alexander et al.*[41], we use the *A*-value to represent the fraction of O_3 oxidation in NO_2 formation:

$$A = \frac{k_1 \cdot [NO] \cdot [O_3]}{k_1 \cdot [NO] \cdot [O_3] + k_2 \cdot [NO] \cdot [HO_2] + k_3 \cdot [NO] \cdot [RO_2]} \quad (1)$$

Where k_1, k_2 and k_3 are the reaction rate constants from *Atkinson et al.*[58]. A smaller *A*-value leads to lower $\Delta^{17}O(NO_2)$ and thus lower $\Delta^{17}O(NO_3^-)$. As shown in Figure 3c, the *A*-values are lower in the glacial period compared to the Holocene in the northern hemisphere. In comparison with the $O_3/(HO_2 + RO_2)$ ratio, the *A*-value also takes into account the effect of changes in the temperature-dependent reaction rate constants between different climates, and thus better estimates the effect of tropospheric chemistry changes on $\Delta^{17}O(NO_3^-)$.

Therefore, if only tropospheric chemistry is taken into account, the *A*-value is expected to decrease from the Holocene to the LGM (Supplementary Table 1). This should lead to lower $\Delta^{17}O(NO_2)$ and thus $\Delta^{17}O(NO_3^-)$ values in the LGM if other factors are the same, opposite to the observed trend in our ice-core observations.

S1.2. The terminal reactions (NO_2 → HNO_3)

Terminal reactions oxidizing NO_2 to HNO_3 can be in general categorized as daytime (OH) and nighttime (O_3) reactions. The relative importance of OH and O_3 for the oxidation of NO_2 to HNO_3 is to first order determined by the length of day versus night, which changes seasonally but does not change over the time scales considered here. The importance of OH and O_3 in the oxidation of NO_2 to HNO_3 is also influenced by the abundances of these oxidants, as well as by the aerosol surface area (influencing the rate of N_2O_5 hydrolysis) and abundance of DMS or VOC (influencing the rate of NO_3 + DMS/VOC). Thus, in addition to the relative abundance of $O_3/(HO_2 + RO_2)$, $\Delta^{17}O(NO_3^-)$ is also influenced by O_3/OH, aerosol surface area, and DMS and VOC concentrations. Although these are of secondary importance relative to $O_3/(HO_2 + RO_2)$, their effects on climate-driven variability in observed $\Delta^{17}O(NO_3^-)$ must be considered. For example, the rate of nitrate formed through N_2O_5 hydrolysis is mainly affected by aerosol composition, surface area, temperature and relative humidity[41,59]. If this pathway increases significantly in the colder climates due to increased atmospheric dust and sea-salt aerosol abundances or decreases in air temperature[60], larger $\Delta^{17}O(NO_3^-)$ would be expected, as is observed. In addition, observations of $\Delta^{17}O(NO_3^-)$ in atmospheric nitrate in the Arctic[42,56] and tropical marine boundary layer[61] suggest that $BrONO_2$ hydrolysis is also a significant nitrate formation pathway, and could even be episodically dominant such as during the polar ozone-depletion events[42]. Increases in $BrONO_2$ hydrolysis in the glacial climate would tend to increase $\Delta^{17}O(NO_3^-)$, as is observed.

In order to estimate changes in the relative importance of the oxidation pathway of NO_2 to nitrate from the Holocene to the glacial period, we use the ICECAP model to estimate changes in the production rates of HNO_3 over the glacial-interglacial time scale due to precursor emissions and chemistry alone. The ICECAP model underestimates the glacial atmospheric sea-salt aerosol

abundance likely due to the lack of a sea-salt aerosol source from the sea-ice surface, which may cause a modeled underestimate of the HNO_3 production rate through N_2O_5 hydrolysis in the glacial period, as well as the concentration of reactive bromine[62] and thus $BrONO_2$ hydrolysis. However, the main NO_x source region for nitrate in Greenland is in the northern mid-latitudes (30-60 °N), where the influence of sea ice on sea salt aerosols is relatively small. In ICECAP, the annual mean production rates of HNO_3 through NO_2 + OH, NO_3 + DMS/VOC, N_2O_5 and $BrONO_2$ hydrolysis, as well as the relative importance (i.e., fraction) of each pathway for annual mean HNO_3 production, in the northern mid-latitudes in each climate scenario are listed in Supplementary Table 1. In ICECAP, the rate of HNO_3 production for all pathways is decreased in the LGM climate compared to the Holocene, mainly due to reduced emissions of NO_x. Additionally, in the extra-tropics, the net decrease in simulated aerosol particle abundances in the cold climates relative to the Holocene decreases N_2O_5 hydrolysis loss frequencies. This decrease in aerosol abundance primarily reflects emission-driven reductions in organic aerosol and its precursors[53], despite increases in mineral dust[63]. Similarly, climate-driven reductions in biogenic DMS and VOC emissions in the cold climates reduce the rate and importance of NO_3 + DMS/VOC. The reduced aerosol abundance in the cold climates also decreases $BrONO_2$ hydrolysis rate, despite increases in BrO concentration in the model.

Since nitrate production rate from all pathways decreased in the LGM compared to the Holocene, the changes in the relative importance of each pathway which influences $\Delta^{17}O(NO_3^-)$ is then determined by the relative degree of decreases in each pathway. As shown in Supplementary Table 1, while the relative importance of NO_2 + OH, N_2O_5 hydrolysis and NO_3 + DMS/VOC in general decreases in the LGM compared to the Holocene, that of $BrONO_2$ hydrolysis increased significantly from the Holocene (~7.7 %) to the LGM (23.1 % and 14.2 %

in the cold and warm LGM, respectively). In ICECAP, the abundance of BrO increases in the LGM compared to the Holocene, primarily due to decreases in HO_2 which is the largest sink of BrO_x (= Br + BrO), in addition to increases in reactive Br production from HOBr photolysis. The increases in BrO concentrations buffer the decreases in $BrONO_2$ hydrolysis rates caused primarily by reduced NO_x emissions and aerosol abundances. This explains why the production from $BrONO_2$ hydrolysis decreases by a smaller degree than the other terminal pathways in the LGM compared to the Holocene. Fractional increases in $BrONO_2$ hydrolysis will tend to increase $\Delta^{17}O(NO_3^-)$ in cold climates, consistent with the observed trend in $\Delta^{17}O(NO_3^-)$.

Using the ICECAP model calculated fraction of each nitrate formation pathway, the $\Delta^{17}O(NO_3^-)$ value is calculated according the following equation:

$$\Delta^{17}O(NO_3^-) = f_1 \cdot \Delta^{17}O_1 + f_2 \cdot \Delta^{17}O_2 + f_3 \cdot \Delta^{17}O_3 + f_4 \cdot \Delta^{17}O_4 \qquad (2)$$

Where f_x and $\Delta^{17}O_x$ represent the fraction and $\Delta^{17}O$ value of each terminal reaction. x = 1, 2, 3, 4, refers to OH oxidation, NO_3 + DMS/VOC reaction, and N_2O_5 and $BrONO_2$ hydrolysis, respectively.

$\Delta^{17}O_x$ is calculated by following equations:

$$\Delta^{17}O_1 = \frac{2}{3} \cdot A \cdot \Delta^{17}O(O_3^*) \qquad (3)$$

$$\Delta^{17}O_2 = \frac{2}{3} \cdot A \cdot \Delta^{17}O(O_3^*) + \frac{1}{3} \cdot \Delta^{17}O(O_3^*) \qquad (4)$$

$$\Delta^{17}O_3 = \frac{4}{6} \cdot A \cdot \Delta^{17}O(O_3^*) + \frac{1}{6} \cdot \Delta^{17}O(O_3^*) \qquad (5)$$

$$\Delta^{17}O_4 = \frac{2}{3} \cdot A \cdot \Delta^{17}O(O_3^*) + \frac{1}{3} \cdot \Delta^{17}O(O_3^*) \qquad (6)$$

Where $\Delta^{17}O(O_3^*)$ is the isotopic anomaly transferred to NO_2 which is approximately 48 ‰ when $\Delta^{17}O$ in bulk $\Delta^{17}O$ is ~35 ‰[52], and *A* is the *A*-value as expressed in Equation (1).

The ICECAP model-calculated mean values of $\Delta^{17}O(NO_3^-)$ in the northern mid- to high-latitudes in each climate scenario are listed in Supplementary Table 1. Due to the decreased *A*-values in the LGM compared to the Holocene, $\Delta^{17}O(NO_3^-)$ in the LGM decreases by 2.5 ‰ to 3.3 ‰, despite the increases in the relative importance of $BrONO_2$ hydrolysis. Modeled increases in the relative importance of $BrONO_2$ hydrolysis alone from the Holocene to LGM increase $\Delta^{17}O(NO_3^-)$ by 2.5 ‰ and 1.0 ‰ in the cold and warm LGM, respectively, partially counteracting decreases in $\Delta^{17}O(NO_3^-)$ driven by decreases in O_3 oxidation relative to HO_x oxidation. The model may underestimate the strength of $BrONO_2$ hydrolysis in the LGM in part because sources of bromine don't change with climate in ICECAP. In order for increases in the relative importance of $BrONO_2$ hydrolysis to explain the observed 6.2 ‰ glacial-interglacial change in the ice-core $\Delta^{17}O(NO_3^-)$ record, it must account for 70 - 82 % of total nitrate production in the northern mid- to high-latitudes in the glacial period. This fraction is large over the broad spatial and temporal scales considered here, as $BrONO_2$ hydrolysis contributes only (20 ± 10) % to total nitrate production even in high halogen environments (i.e., tropical marine boundary layer) in the present day atmosphere[44]. In the polar regions after polar sunrise when O_3 depletion events occur[64], $BrONO_2$ hydrolysis may dominate local nitrate production[42]. However, these short-lived episodes are constrained to polar springtime and do not represent the major nitrate production pathways over the larger spatial and temporal scales currently recorded in Greenland ice cores.

In sum, although the relative importance of $BrONO_2$ hydrolysis for nitrate production in the LGM may contribute to the observed glacial increase in $\Delta^{17}O(NO_3^-)$, it is unlikely that increases in $BrONO_2$ hydrolysis alone can explain the magnitude of the observed change in $\Delta^{17}O(NO_3^-)$ between the Holocene and the LGM. However, the direction and magnitude of the

sensitivity of reactive halogen chemistry to climate has not been explored, and changes in reactive halogen chemistry may play an important role in the observed trend in $\Delta^{17}O(NO_3^-)$**.**

S.2. The effects of stratospheric-sourced O_3 from STT

An additional source of O_3 from the stratosphere through Stratosphere-to-Troposphere Transport (STT) will tend to increase $\Delta^{17}O(NO_3^-)$ through 1) increasing the *A*-value, and 2) enhancing the relative importance of pathways that produce nitrate with larger $\Delta^{17}O(NO_3^-)$, i.e., the nighttime reactions and $BrONO_2$ hydrolysis. Changes in total O_3 concentrations would affect the steady-state concentration of NO_2, and thus the production rates of HNO_3 from all of the terminal reactions. However, since all terminal reactions would be enhanced by the same factor due to the increased NO_2 concentration assuming a linear response, the relative contribution of each terminal reaction should then stay the same and no effect on $\Delta^{17}O(NO_3^-)$ should be expected. In contrast, increases in total O_3 concentration will enhance the nighttime reactions (NO_3 + DMS/VOC and N_2O_5 hydrolysis) through promoting NO_3 production by $NO_2 + O_3$, and $BrONO_2$ hydrolysis through promoting BrO production by $Br + O_3$, while not directly influencing NO_2 + OH oxidation. Therefore, increases in total O_3 concentrations in the troposphere will increase $\Delta^{17}O(NO_3^-)$ by increasing the *A*-value and by increasing the relative importance of nighttime reactions and $BrONO_2$ hydrolysis, assuming HO_x is relatively constant. Our multiple model sensitivity studies suggest that over major climate transitions[53,65], production of total HO_x (OH + HO_2 + RO_2) is most sensitive to O_3 photolysis frequencies (influenced by stratospheric O_3 column abundance which determines the surface UV levels) and water vapor abundances. It is less sensitive to tropospheric ozone concentrations ($[O_3]$) because (1) photolysis frequency variability in space and time is much greater than tropospheric $[O_3]$ variability, (2) OH production is also limited by water vapor abundance (most O^1D is immediately quenched back to

O_3), and (3) water vapor abundance is dominated by physical processes (e.g., evaporation rate) and thus independent of O_3 abundance. The partitioning of HO_x between $HO_2 + RO_2$ and OH is then set by the relative abundances of NO to VOCs and CO. Therefore, chemical factors other than tropospheric ozone abundances exert greater influences on tropospheric ($HO_2 + RO_2$), and therefore O_3 and ($HO_2 + RO_2$) do not necessarily co-vary in time.

We do however note that the strength of the Brewer-Dobson Circulation (BDC), through which STT is largely affected, influences the spatial distribution of stratospheric ozone and hence UV levels in the troposphere. Therefore, all else being equal, with a stronger BDC in the glacial climate, surface UV levels will decrease in the mid- to high-latitudes and increase in the tropics. This should further reduce the total HO_x production in the mid- to high-latitudes, and thus $HO_2 + RO_2$ abundances in the northern mid- to high-latitudes assuming all other factors are the same. This also tends to increase the tropospheric $O_3/(HO_2+RO_2)$ ratio, in addition to direct stratospheric O_3 input, consistent with the observations of increased $\Delta^{17}O(NO_3^-)$ in the glacial time.

In summary, if the stratospheric-sourced O_3 is enhanced in the LGM compared to the Holocene, $\Delta^{17}O(NO_3^-)$ in the LGM will be increased, qualitatively consistent with the observations. In the section that follows, we estimate the required increases in stratospheric-sourced O_3 through STT from the Holocene to the LGM in order to explain the observed 6.2 ‰ glacial-interglacial difference in $\Delta^{17}O(NO_3^-)$.

S.3. The required increase in stratospheric-sourced O_3 to explain the observations

In order to estimate the increase in stratospheric-sourced O_3 required to explain the observed increase in glacial $\Delta^{17}O(NO_3^-)$, we define λ as the ratio of total O_3 in the troposphere to O_3 originating from *in-situ* production only:

$$\lambda = \frac{[O_3]_i + [O_3]_{strat}}{[O_3]_i} \quad (7)$$

where $[O_3]_i$ represent *in-situ* O_3 concentration and $[O_3]_{strat}$ represents the concentration of stratospheric-sourced O_3.

The *A*-value from equation 1 becomes:

$$A = \frac{k_1 \cdot [NO] \cdot [O_3]_i \cdot \lambda}{k_1 \cdot [NO] \cdot [O_3]_i \cdot \lambda + k_2 \cdot [NO] \cdot [HO_2] + k_3 \cdot [NO] \cdot [RO_2]} \quad (8)$$

Assuming a linear response to increases in total O_3 concentrations in the troposphere, the production rates of nighttime reactions (i.e., NO_3 + DMS/VOC and N_2O_5 hydrolysis) and $BrONO_2$ hydrolysis would be enhanced by a factor of "λ" relative to the values reported in Supplementary Table 1. Subsequently, f_x, i.e., the fraction of each nitrate production pathway relative to total nitrate production, is a function of "λ".

In order to explain the observed 6.2 ‰ glacial-interglacial difference in $\Delta^{17}O(NO_3^-)$, we need:

$$6.2‰ = \Delta^{17}O(NO_3^-)_{LGM} - \Delta^{17}O(NO_3^-)_H \quad (9)$$

Where 'LGM' represents WB or CM (the cold or warm LGM climate, respectively) and H represents the Holocene.

Substituting equations (3)-(6) into equation (2), we obtain:

$$\Delta^{17}O(NO_3^-)_H = \frac{2}{3} \cdot A_H \cdot \Delta^{17}O(O_3^*) + \frac{1}{3} \cdot \Delta^{17}O(O_3^*) \cdot (f_{2\_H} + f_{4\_H}) + \frac{1}{6} \cdot \Delta^{17}O(O_3^*) \cdot f_{3\_H} \quad (10)$$

$$\Delta^{17}O(NO_3^-)_{LGM} = \frac{2}{3} \cdot A_{LGM} \cdot \Delta^{17}O(O_3^*) + \frac{1}{3} \cdot \Delta^{17}O(O_3^*) \cdot (f_{2\_LGM} + f_{4\_LGM}) + \frac{1}{6} \cdot \Delta^{17}O(O_3^*) \cdot f_{3\_LGM} \quad (11)$$

Where f_{x_H} and f_{x_LGM} represent the fractional importance of each nitrate production pathway in the Holocene and LGM respectively, and (x = 2, 3, 4) are the terminal reaction

pathways NO_3 + DMS/VOC, N_2O_5 hydrolysis and $BrONO_2$ hydrolysis, respectively. f_{x_H} and f_{x_LGM} are functions of λ_H and λ_{LGM}, respectively:

$$f = \frac{R2 \cdot \lambda}{R1 + \lambda \cdot (R2 + R3 + R4)} \qquad (12)$$

where R1-R4 represent the production rate of each terminal nitrate formation pathway, as shown in Supplementary Table 1.

Substituting equations (8) and (12) into (10) and (11), and combining the resulting equations with equation (9), we get one equation with two unknowns, λ_H and λ_{LGM}. All other terms are calculated in ICECAP. This equation is simplified as the following:

$$6.2‰ = \mathrm{F}(\lambda_{\mathrm{LGM}}) - \mathrm{F}(\lambda_{\mathrm{H}}) \qquad (13)$$

Where $F(\lambda_{LGM})$ and $F(\lambda_H)$ are functions of the unknown terms λ_{LGM} and λ_H, respectively.

Assuming that the stratosphere to troposphere flux of O_3 has not changed significantly over the industrial era, we can use present-day stratospheric-sourced O_3 to represent $[O_3]_{strat\_H}$. In ICECAP, the present day annual mean tropospheric O_3 concentration originating from the stratosphere in the northern mid- to high-latitudes is 0.32×10^{12} molecule/cm^3 (13.6 ppbv), representing ~ 22 % of total ozone concentration in this region over the entire troposphere. This fraction is within the range of stratospheric contribution to tropospheric ozone estimated by other models (e.g., *Hess and Lamarque*[66], and *Hess et al.*[67]).

$[O_3]_{i\_H}$ in ICECAP is 0.49×10^{12} molecule/cm^3 (20.8 ppbv), so that λ_H is 1.66 according to equation (7). The *A*-value in the Holocene from the ICECAP model and calculated in Equation (8) is $A_H = 0.74$, compared to 0.65 when including only *in-situ* produced O_3 in the troposphere. Including both stratospheric-sourced O_3 and *in-situ* produced O_3 in the troposphere, the

calculated mean $\Delta^{17}O(NO_3^-)$ value northern mid- to high-latitudes in the Holocene is 28.9 ‰, which is consistent with the observed $\Delta^{17}O(NO_3^-)$ value of (29.4 ± 0.7) ‰ in the Holocene.

With known λ_H = x, we can then solve equation (13) for λ_{LGM}, resulting in values of λ_{LGM} = 4.10 and 3.29 for the warm and cold LGM, respectively. In ICECAP, tropospheric, annual-mean $[O_3]_i$ is 0.36 and 0.30 molecule/cm^3 (15.5 and 12.8 ppbv) for the warm and cold LGM, respectively, in the northern mid- to high-latitudes. According to equation (7), $[O_3]_{strat}$ is then 1.12 and 0.69 molecule/cm^3 (47.9 and 29.5 ppbv) in the warm and cold LGM in this region, respectively, representing 75.6 % and 69.7 % of the total tropospheric ozone abundance in each glacial scenario. We then can calculate the changes in stratospheric-sourced O_3 between the LGM and Holocene using the following equation:

$$z = \frac{[O_3]_{s\_LGM} - [O_3]_{s\_H}}{[O_3]_{s\_H}} \qquad (14)$$

where 'z' represents the fractional change in stratospheric-sourced O_3 from the LGM to the Holocene. Equation 14 yields z = 252 % and 118 % for the warm and cold LGM climate, respectively. This means that the tropospheric concentration of stratospheric-sourced O_3 must increase by 251 % and 118 % in the warm and cold LGM compared to the Holocene, respectively, in the northern mid-to high-latitudes, in order to explain the entirety of the observed change in $\Delta^{17}O(NO_3^-)$. The calculated stratospheric-sourced O_3 is higher in the warm LGM than the cold LGM. This is because the relative importance of $BrONO_2$ hydrolysis is increased more in the cold than warm LGM (Supplementary Table 1), leading to less stratospheric-soured O_3 needed to explain the ice core $\Delta^{17}O(NO_3^-)$ record.

We note, however, the calculated 118-252 % increase in stratospheric-sourced O_3 through STT from the Holocene to LGM is probably a high-end estimate. The chemistry simulated by

ICECAP may underestimate the role of N_2O_5 and $BrONO_2$ hydrolysis in the LGM due to the lack of a sea-salt aerosol source from the sea ice. Sea salt aerosols promote N_2O_5 and $BrONO_2$ hydrolysis and is also important for the production of reactive bromine which leads to $BrONO_2$. Additionally, and increased BDC in cold climates will tend to increase the stratospheric O_3 column abundance in the mid- to high-latitudes, resulting in a decreased HO_x production rate and an increased O_3/HO_x ratio. In sum, there are large uncertainties regarding the magnitude of our estimated increase in stratospheric-sourced O_3, and we expect that our calculated 118-252 % increase in stratospheric-sourced O_3 is an upper limit. However, the observed glacial interglacial variability in $\Delta^{17}O(NO_3^-)$ is difficult to explain from tropospheric chemistry alone. More observational and modeling work is needed to reduce the uncertainty. We also note the estimated increase in stratospheric-sourced O_3 may be a result of a variety of processes, caused not only by an enhanced BDC but also increased stratospheric O_3 abundance due to lower CH_4 and N_2O abundances in the glacial climate, and/or increases in synoptic-scale processes such as tropopause folding events[68-69]. More research is required to examine the causes, and to assess the magnitude, of the observed increases in STT in the glacial climate.

S4. Other potential factors influencing $\Delta^{17}O(NO_3^-)$

S4.1. Effects of post-depositional processing of snow nitrate on GISP2 $\Delta^{17}O(NO_3^-)$

Post-depositional processing of snow nitrate occurs in the air-snow interface, and includes evaporation or desorption of HNO_3 from snow and the UV photolysis of snow nitrate[70-71]. The latter is recognized as the main process influencing the preservation of nitrate and its isotopic signal in snow and ice cores[72-73]. The main photo-product, NO_x, is quickly transported from the snowpack to the overlying atmosphere through wind pumping[74-76], where it is re-oxidized to nitrate. Reformation of nitrate from the photo-products in the condensed phase of snow grains

(i.e., the disorganized layer of snow grain surface) also occurs if the nitrate being photolyzed is trapped inside the snow grain instead of on its surface[77].

The recycling in the air-snow interface replaces the regional atmospheric $\Delta^{17}O(NO_3^-)$ signal with a local signal by reforming nitrate under local tropospheric oxidant conditions. Because UV photolysis of snow nitrate only happens during periods of sunlight (mainly in the summer months), this tends to lower $\Delta^{17}O$ in the reformed nitrate compared to the originally deposited nitrate[78], but overall the snow $\Delta^{17}O(NO_3^-)$ still represents atmospheric conditions. In contrast, recycling in the condensed phase erases the atmospheric signal preserved in $\Delta^{17}O(NO_3^-)$ by exchanging oxygen atoms with water that possesses zero $\Delta^{17}O$, and therefore forms nitrate with very low $\Delta^{17}O(NO_3^-)$ compared with the originally deposited nitrate[72]. The degree of post-depositional processing of snow nitrate is influenced mainly by surface UV intensity, snow accumulation rate, and snow UV light-absorbing impurities (UV-LAI) (e.g., organics, dust and black carbon)[73,76,79]. Field observations from East Antarctic snowpits[72] indicate that at sites with snow accumulation rates greater than 0.1 m ice a^{-1}, the effect of nitrate recycling in the condensed phase on snow $\Delta^{17}O(NO_3^-)$ is negligible under present day Antarctic snow UV-LAI concentrations. The reason seems to be that nitrate trapped inside snow grains will not be effectively photolyzed until the snow stays in the photic zone long enough so that photolabile nitrate is attenuated[77].

For the GISP2 ice core, the snow accumulation rate falls below 0.1 m ice a^{-1} frequently during the glacial climate (Figure 2b). This appears to suggest that $\Delta^{17}O(NO_3^-)$ in the GISP2 ice core may lose its atmospheric signal by some degree in the glacial climate. However, in the glacial period, snow UV-LAI concentrations are much higher than that in Antarctic snow in the present day[60] which tends to decrease the depth of the photic zone and will limit recycling in the

condensed phase by lowering the amount of time snow nitrate spends in the snow photic zone. This is evident by the $\delta^{15}N(NO_3^-)$ record from the GISP2 ice core[80]. The highest glacial $\delta^{15}N(NO_3^-)$ value in GISP2 core (38.9 ± 0.3‰) is equivalent to the asymptotic $\delta^{15}N(NO_3^-)$ value (the value after nitrate is buried below the photic zone)[72] at sites with snow accumulation rates of 0.12 - 0.16 m ice a^{-1}. This suggests that in the glacial period, even though snow accumulation rates at Summit sometimes fall below 0.1 m ice a^{-1} over the time period reported here, nitrate recycling in the condensed phase is negligible due to the shallower photic zone caused by higher LAI concentrations.

In addition, based on the record of $\delta^{15}N(NO_3^-)$ in the GISP2 ice core[80], we have estimated that the degree of post-depositional processing of snow nitrate is greater in the last glacial period compared to the Holocene. This effect alone will drive $\Delta^{17}O(NO_3^-)$ to be lower in the glacial period compared to the Holocene, which is the opposite of what is observed. Therefore, trends in the $\Delta^{17}O(NO_3^-)$ record from the GISP2 ice core over the time periods considered here cannot be the result of changes in post-depositional processing. It is however possible that the higher degree of post-depositional processing in the glacial climate is muting the effect of changes in oxidants on the record, making the observed changes in $\Delta^{17}O(NO_3^-)$ a lower limit proxy for climate-driven variability in oxidant abundances.

S4.2. Potential effects of stratospheric denitrification

Stratospheric denitrification refers to the sedimentation process of Polar Stratospheric Clouds (PSCs) containing nitric acid trihydrate. Research on nitrate in Antarctic snow[81] has suggested that stratospheric denitrification associated with the winter polar vortex could result in a late winter/early spring nitrate concentration maximum in snow. This is supported by measurements of $\Delta^{17}O(NO_3^-)$ in the boundary layer and surface snow in East Antarctica[82], which

show a strong influence of stratospheric nitrate which possesses higher $\Delta^{17}O(NO_3^-)$ than nitrate formed in the troposphere. In the present climate, due to the warmer winter and the weaker and less persistent Arctic vortex compared to Antarctica, denitrification occurs less frequently and less extensively in the Arctic[83]. There is currently no observational evidence that suggests that significant stratospheric nitrate input occurs in the Arctic troposphere, consistent with model simulations that the stratospheric contribution of nitrate to Greenland is negligible[41].

In the glacial period, due to decreased greenhouse gas burdens, the stratosphere is predicted to be warmer than the Holocene, and with a weaker polar vortex compared to today[84] despite dynamical changes in atmospheric circulation in the northern high latitudes due to the growth of continental ice sheet. Thus, the contribution of stratospheric nitrate to Greenland is expected to be weaker in the glacial period compared to the Holocene. This will tend to lower ice-core $\Delta^{17}O(NO_3^-)$ in the glacial period, opposite to the observations. Thus, it is unlikely that variability in stratospheric denitrification in the Arctic can explain the observed variability in $\Delta^{17}O(NO_3^-)$ reported here.

Supplementary Table 1. Annual mean production rate and fraction of each terminal reaction from NO_2 to HNO_3, the *A*-value and the calculated $\Delta^{17}O(NO_3^-)$ value in northern mid-to high-latitudes in each climate scenario predicted by ICECAP, using tropospheric O_3 from *in situ* production only (i.e., the effect of stratospheric-sourced ozone is not included).

	OH oxidation		NO_3 +DMS/VOC		N_2O_5 hydrolysis		$BrONO_2$ hydrolysis		*A*-value	$\Delta^{17}O$ (NO_3^-) (‰)
	molec·cm^{-3}·s^{-1}	**(%)**	molec·cm^{-3}·s^{-1}	**(%)**	molec·cm^{-3}·s^{-1}	**(%)**	molec·cm^{-3}·s^{-1}	**(%)**		
Holocene	4085.9	**72.6**	605.0	**10.8**	500.4	**8.9**	434.1	**7.7**	0.65 (*0.74*)[a]	24.4 (*28.9*)
Cold-LGM	426.7	**64.3**	67.6	**10.2**	15.8	**2.4**	153.5	**23.1**	0.51 (*0.79*)	21.9 (*35.1*)
Warm-LGM	871.2	**73.8**	108.9	**9.29**	32.9	**2.8**	166.2	**14.2**	0.54 (*0.82*)	21.1 (*35.1*)

[a]Values in parenthesis are the calculated *A*-value and $\Delta^{17}O(NO_3^-)$ with the effects of STT of O_3.

References:

40 Levy, H., Moxim, W. J., Klonecki, A. A. & Kasibhatla, P. S. Simulated tropospheric NO_x: Its evaluation, global distribution and individual source contributions. *J. Geophys. Res.* **104**, 26279-26306, doi:10.1029/1999JD900442 (1999).

41 Alexander, B. *et al.* Quantifying atmospheric nitrate formation pathways based on a global model of the oxygen isotopic composition ($\Delta^{17}O$) of atmospheric nitrate. *Atmos. Chem. Phys.* **9**, 5043-5056, doi:10.5194/acp-9-5043-2009 (2009).

42 Morin, S., Savarino, J., Bekki, S., Gong, S. & Bottenheim, J. W. Signature of Arctic surface ozone depletion events in the isotope anomaly ($\Delta^{17}O$) of atmospheric nitrate. *Atmos. Chem. Phys.* **7**, 1451-1469, doi:10.5194/acp-7-1451-2007 (2007).

43 Evans, M. J. *et al.* Coupled evolution of BrOx-ClOx-HOx-NOx chemistry during bromine-catalyzed ozone depletion events in the arctic boundary layer. *J. Geophys. Res.* **108**, 2156-2202, doi:10.1029/2002jd002732 (2003).

44 Savarino, J. *et al.* Isotopic composition of atmospheric nitrate in a tropical marine boundary layer. *Proc. Natl. Acad. Sci.* **110**, 17668-17673, doi:10.1073/pnas.1216639110 (2013).

45 Lyons, J. R. Transfer of mass-independent fractionation in ozone to other oxygen-containing radicals in the atmosphere. *Geophys. Res. Lett.* **28**, 3231-3234, doi:10.1029/2000GL012791 (2001).

46 Gao, Y. Q., Chen, W. C. & Marcus, R. A. A theoretical study of ozone isotopic effects using a modified ab initio potential energy surface. *J Chem Phys* **117**, 1536-1543, doi:10.1063/1.1488577 (2002).

47 Alexander, B. & Mickley, L. Paleo-Perspectives on Potential Future Changes in the Oxidative Capacity of the Atmosphere Due to Climate Change and Anthropogenic Emissions. *Curr Pollution Rep*, 1-13, doi:10.1007/s40726-015-0006-0 (2015).

48 Hastings, M. G., Sigman, D. M. & Steig, E. J. Glacial/interglacial changes in the isotopes of nitrate from the Greenland Ice Sheet Project 2 (GISP2) ice core. *Global Biogeochem. Cy.* **19**, GB4024, doi:10.1029/2005gb002502 (2005).

49 Vicars, W. C. & Savarino, J. Quantitative constraints on the 17O-excess (Δ17O) signature of surface ozone: Ambient measurements from 50 ºN to 50 ºS using the nitrite-coated filter technique. *Geochim Cosmochim Ac* **135**, 270-287, doi:http://dx.doi.org/10.1016/j.gca.2014.03.023 (2014).

50 Vicars, W. C., Bhattacharya, S. K., Erbland, J. & Savarino, J. Measurement of the 17O-excess (Δ17O) of tropospheric ozone using a nitrite-coated filter. *Rapid Commun. Mass Spectrom.* **26**, 1219-1231, doi:10.1002/rcm.6218 (2012).

51 Johnston, J. C. & Thiemens, M. H. The isotopic composition of tropospheric ozone in three environments. *J. Geophys. Res.* **102**, 25395-25404 (1997).

52 Michalski, G., Bhattacharya, S. K. & Girsch, G. NOx cycle and the tropospheric ozone isotope anomaly: an experimental investigation. *Atmos. Chem. Phys.* **14**, 4935-4953, doi:10.5194/acp-14-4935-2014 (2014).

53 Murray, L. T. *et al.* Factors controlling variability in the oxidative capacity of the troposphere since the Last Glacial Maximum. *Atmos. Chem. Phys.* **14**, 3589-3622, doi:10.5194/acp-14-3589-2014 (2014).

54 Kaplan, J. O., Folberth, G. & Hauglustaine, D. A. Role of methane and biogenic volatile organic compound sources in late glacial and Holocene fluctuations of atmospheric methane concentrations. *Global Biogeochem. Cy.* **20**, doi:10.1029/2005GB002590 (2006).

55 Martinerie, P., Brasseur, G. P. & Granier, C. The chemical composition of ancient atmospheres: A model study constrained by ice core data. *Journal of Geophysical Research: Atmospheres* **100**, 14291-14304, doi:10.1029/95jd00826 (1995).

56 Morin, S. *et al.* Tracing the Origin and Fate of NO_x in the Arctic Atmosphere Using Stable Isotopes in Nitrate. *Science* **322**, 730-732, doi:10.1126/science.1161910 (2008).

57 Morin, S., Savarino, J., Bekki, S., Gong, S. & Bottenheim, J. W. Signature of Arctic surface ozone depletion events in the isotope anomaly ($\Delta^{17}O$) of atmospheric nitrate. *Atmos. Chem. Phys.* **7**, 1451-1469, doi:10.5194/acp-7-1451-2007 (2007).
58 Atkinson, R. *et al.* Evaluated kinetic and photochemical data for atmospheric chemistry: Volume I - gas phase reactions of Ox, HOx, NOx and SOx species. *Atmos. Chem. Phys.* **4**, 1461-1738, doi:10.5194/acp-4-1461-2004 (2004).
59 Griffiths, P. T. & Anthony Cox, R. Temperature dependence of heterogeneous uptake of N2O5 by ammonium sulfate aerosol. *Atmospheric Science Letters* **10**, 159-163, doi:10.1002/asl.225 (2009).
60 Mayewski, P. A. *et al.* Major features and forcing of high-latitude northern hemisphere atmospheric circulation using a 110,000-year-long glaciochemical series. *J. Geophys. Res.* **102**, 26345-26366, doi:10.1029/96jc03365 (1997).
61 Savarino, J. *et al.* Isotopic composition of atmospheric nitrate in a tropical marine boundary layer. *Proc. Natl. Acad. Sci.* , doi:10.1073/pnas.1216639110 (2013).
62 Yang, X., Pyle, J. A. & Cox, R. A. Sea salt aerosol production and bromine release: Role of snow on sea ice. *Geophys. Res. Lett.* **35**, doi:10.1029/2008gl034536 (2008).
63 Mahowald, N. M. *et al.* Climate response and radiative forcing from mineral aerosols during the last glacial maximum, pre-industrial, current and doubled-carbon dioxide climates. *Geophys. Res. Lett.* **33**, L20705, doi:10.1029/2006gl026126 (2006).
64 Barrie, L. A., Bottenheim, J. W., Schnell, R. C., Crutzen, P. J. & Rasmussen, R. A. Ozone destruction and photochemical reactions at polar sunrise in the lower Arctic atmosphere. *Nature* **334**, 138-141, doi:10.1038/334138a0 (1988).
65 Achakulwisut, P. *et al.* Uncertainties in isoprene photochemistry and emissions: implications for the oxidative capacity of past and present atmospheres and for climate forcing agents. *Atmos. Chem. Phys.* **15**, 7977-7998, doi:10.5194/acp-15-7977-2015 (2015).
66 Hess, P. G. & Lamarque, J.-F. Ozone source attribution and its modulation by the Arctic oscillation during the spring months. *Journal of Geophysical Research: Atmospheres* **112**, n/a-n/a, doi:10.1029/2006jd007557 (2007).
67 Hess, P. G. & Zbinden, R. Stratospheric impact on tropospheric ozone variability and trends: 1990–2009. *Atmos. Chem. Phys.* **13**, 649-674, doi:10.5194/acp-13-649-2013 (2013).
68 Sprenger, M., Wernli, H. & Bourqui, M. Stratosphere–Troposphere Exchange and Its Relation to Potential Vorticity Streamers and Cutoffs near the Extratropical Tropopause. *J. Atmos. Sci.* **64**, 1587-1602, doi:doi:10.1175/JAS3911.1 (2007).
69 Xie, B., Zhang, H., Wang, Z., Zhao, S. & Fu, Q. A modeling study of effective radiative forcing and climate response due to tropospheric ozone. *Adv Atmos Sci* **33**, 819-828, doi:10.1007/s00376-016-5193-0 (2016).
70 Röthlisberger, R. *et al.* Nitrate in Greenland and Antarctic ice cores: a detailed description of post-depositional processes. *Ann. Glaciol.* **35**, 209-216, doi:10.3189/172756402781817220 (2002).
71 Wolff, E. W., Jones, A. E., Bauguitte, S. J. B. & Salmon, R. A. The interpretation of spikes and trends in concentration of nitrate in polar ice cores, based on evidence from snow and atmospheric measurements. *Atmos. Chem. Phys.* **8**, 5627-5634, doi:10.5194/acp-8-5627-2008 (2008).
72 Erbland, J. *et al.* Air-snow transfer of nitrate on the East Antarctic Plateau - Part 1: Isotopic evidence for a photolytically driven dynamic equilibrium in summer. *Atmos. Chem. Phys.* **13**, 6403-6419, doi:10.5194/acp-13-6403-2013 (2013).
73 Frey, M. M., Savarino, J., Morin, S., Erbland, J. & Martins, J. M. F. Photolysis imprint in the nitrate stable isotope signal in snow and atmosphere of East Antarctica and implications for reactive nitrogen cycling. *Atmos. Chem. Phys.* **9**, 8681-8696, doi:10.5194/acp-9-8681-2009 (2009).

74 Honrath, R. E. *et al.* Evidence of NO_x production within or upon ice particles in the Greenland snowpack. *Geophys. Res. Lett.* **26**, 695-698, doi:10.1029/1999GL900077 (1999).
75 Thomas, J. L. *et al.* Modeling chemistry in and above snow at Summit, Greenland - Part 2: Impact of snowpack chemistry on the oxidation capacity of the boundary layer. *Atmos. Chem. Phys.* **12**, 6537-6554, doi:10.5194/acp-12-6537-2012 (2012).
76 Zatko, M. C. *et al.* The influence of snow grain size and impurities on the vertical profiles of actinic flux and associated NO_x emissions on the Antarctic and Greenland ice sheets. *Atmos. Chem. Phys.* **13**, 3547-3567, doi:10.5194/acp-13-3547-2013 (2013).
77 Meusinger, C., Berhanu, T. A., Erbland, J., Savarino, J. & Johnson, M. S. Laboratory study of nitrate photolysis in Antarctic snow. I. Observed quantum yield, domain of photolysis, and secondary chemistry. *J Chem Phys* **140**, doi:10.1063/1.4882898 (2014).
78 Geng, L. *et al.* On the origin of the occasional spring nitrate peak in Greenland snow. *Atmos. Chem. Phys.* **14**, 13361-13376, doi:10.5194/acp-14-13361-2014 (2014).
79 France, J. L. *et al.* Snow optical properties at Dome C (Concordia), Antarctica; implications for snow emissions and snow chemistry of reactive nitrogen. *Atmos. Chem. Phys.* **11**, 9787-9801, doi:10.5194/acp-11-9787-2011 (2011).
80 Geng, L. *et al.* Effects of postdepositional processing on nitrogen isotopes of nitrate in the Greenland Ice Sheet Project 2 ice core. *Geophys. Res. Lett.*, 2015GL064218, doi:10.1002/2015gl064218 (2015).
81 Mulvaney, R. & Wolff, E. W. Evidence for Winter Spring Denitrification of the Stratosphere in the Nitrate Record of Antarctic Firn Cores. *J. Geophys. Res.* **98**, 5213-5220, doi:10.1029/92JD02966 (1993).
82 Savarino, J., Kaiser, J., Morin, S., Sigman, D. M. & Thiemens, M. H. Nitrogen and oxygen isotopic constraints on the origin of atmospheric nitrate in coastal Antarctica. *Atmos. Chem. Phys.* **7**, 1925-1945 (2007).
83 Waugh, D. W. & Randel, W. J. Climatology of arctic and antarctic polar vortices using elliptical diagnostics. *J. Atmos. Sci.* **56**, 1594-1613 (1999).
84 Rind, D., Chandler, M., Lonergan, P. & Lerner, J. Climate change and the middle atmosphere 5. Paleostratosphere in cold and warm climates. *J. Geophys. Res.* **106**, 20195-20212, doi:10.1029/2000jd900548 (2001).